Development and In Vivo Evaluation of a κ-Opioid Receptor Agonist as a PET Radiotracer with Superior Imaging Characteristics

Songye Li, Ming-Qiang Zheng, Mika Naganawa, Sujin Kim, Hong Gao, Michael Kapinos, David Labaree, and Yiyun Huang

PET Center, Yale University School of Medicine, New Haven, Connecticut

Studies have shown κ-opioid receptor (KOR) abnormalities in addictive disorders, other central nervous system diseases, and Alzheimer's disease. We have developed the first set of agonist ^{11}C-GR103545 and antagonist ^{11}C-LY2795050 radiotracers for PET imaging of KOR in humans. Nonetheless, ^{11}C-GR103545 displays protracted uptake kinetics and is not an optimal radiotracer. Here, we report the development and evaluation of ^{11}C-methyl-(*R*)-4-(2-(3,4-dichlorophenyl)acetyl)-3-((diethylamino)methyl)piperazine-1-carboxylate (^{11}C-EKAP) and its comparison with ^{11}C-GR103545. **Methods:** EKAP was synthesized and assayed for in vitro binding affinities and then radiolabeled. PET studies were performed on rhesus monkeys. Blocking studies were performed with naloxone and the selective KOR antagonists LY2795050 and LY2456302. Arterial input functions were generated for use in kinetic modeling. Brain TACs were analyzed with multilinear analysis 1 to derive binding parameters. **Results:** EKAP has high KOR affinity (inhibition constant, 0.28 nM) and good selectivity in vitro. ^{11}C-EKAP was prepared in good radiochemical purity. ^{11}C-EKAP rapidly metabolized in plasma and displayed fast and reversible kinetics in brain, with peak uptake at less than 20 min after injection. Preblocking with naloxone (1 mg/kg) or LY2795050 (0.2 mg/kg) produced 84%–89% receptor occupancy, whereas LY2456302 (0.05 and 0.3 mg/kg) dose-dependently reduced ^{11}C-EKAP–specific binding, thus demonstrating its binding specificity and selectivity in vivo. Mean multilinear analysis 1–derived nondisplaceable binding potential values were 1.74, 1.79, 1.46, 0.80, and 0.77 for cingulate cortex, globus pallidus, insula, striatum, and frontal cortex, respectively, consistent with the known KOR distribution in primate brains. **Conclusion:** We have successfully developed ^{11}C-EKAP as a KOR agonist tracer with dual attractive imaging properties of fast uptake kinetics and high specific binding in vivo.

Key Words: ^{11}C-EKAP; kappa opioid receptor; agonist; PET radiotracer; nonhuman primates

J Nucl Med 2019; 60:1023–1030
DOI: 10.2967/jnumed.118.220517

Received Oct. 1, 2018; revision accepted Dec. 6, 2018.
For correspondence or reprints contact: Songye Li, Yale PET Center, P.O. Box 208048, New Haven, CT 06520.
E-mail: songye.li@yale.edu
Published online Jan. 10, 2019.

Interest in opioids has been sustained over the past few decades since the identification of opioid receptors (*1*) with 3 major subtypes: the morphine-preferring μ-opioid receptor (MOR), the dynorphin-preferring κ-opioid receptor (KOR), and the enkephalin-preferring δ-opioid receptor (DOR) (*2*). In the human brain, KOR has a wide and distinct distribution in the neocortex, striatum, thalamus, amygdala, and hippocampus (*3,4*) and is implicated in the pathophysiology of depression, anxiety, and alcoholism (*5–7*). Early studies of KOR agonists have showed that they induce a significant analgesic effect without the side effects associated with MOR agonists, especially drug dependence and, thus, the potential for abuse (*8*). Increasing evidence indicates that KOR may also be involved in many other disorders, such as epilepsy (*9*), Tourette syndrome (*10*), and Alzheimer's disease (*11*). Visualization, characterization, and quantification of KOR with in vivo imaging techniques such as PET would greatly facilitate the understanding of KOR and its involvement in diseases and their treatment.

A few KOR agonists have been evaluated as PET radiotracers over the past few decades (Fig. 1). U-50488 (*12*) was an early structural lead of potent KOR selective agonists that propagated a large family of derivatives, such as U-69593 (*13*), GR-45809, GR-89896, and GR103545 (*14,15*). The KOR agonists that have been radiolabeled include U50488 and its fluoroalkyl derivatives (*16,17*) GR89696 and GR103545 (*18,19*). Highly potent salvinorin A was isolated from the plant *Salvia divinorum* as a nonalkaloid KOR agonist (*20*) and was radiolabeled (*21*). However, salvinorin A and its derivatives are not suitable candidates for PET radiotracers because of their extremely fast metabolism and tissue kinetics (*21–23*).

KOR belongs to the superfamily of G-protein–coupled receptors. According to the 2-state theory of G-protein–coupled receptor activation (*24*), agonists bind with high affinity to, and interact with, only the active state of the receptor, whereas antagonists bind with equal affinity to both the active and inactive states. An agonist PET radiotracer affords a way to interrogate the active state of a receptor, to assess the ratio of receptors configured in active versus inactive states, and to probe the possible shift of this ratio under diseased conditions (*25*). Indeed, the crystal structure of the single-domain antibody–stabilized KOR active state recently revealed remarkable conformation and binding pocket changes between the active and inactive states (*26*). Hence, the development of a suitable KOR agonist tracer would enable the investigation of receptor state changes in various disorders.

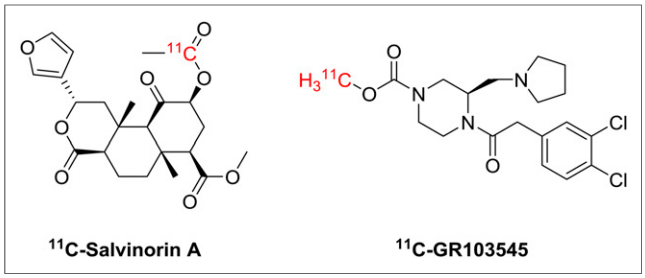

FIGURE 1. Examples of KOR agonist radioligands.

We have developed ^{11}C-GR103545 as a KOR agonist radiotracer for PET imaging applications in nonhuman primates and humans (*27–29*). Although ^{11}C-GR103545 was found to possess appropriate kinetic and imaging properties in baboons (*30*), in humans it displays slow tissue kinetics, which makes quantitative kinetic modeling difficult, with poor test–retest variability in binding parameters.

In our continued effort to find an appropriate KOR agonist radiotracer, we have prepared and evaluated a series of compounds generated by modification of the GR103545 structure. In this article, we report the identification, development, and in vivo evaluation of a KOR agonist radiotracer, ^{11}C-methyl-(*R*)-4-(2-(3,4-dichlorophenyl)acetyl)-3-((diethylamino)methyl)piperazine-1-carboxylate (^{11}C-EKAP), with improved pharmacokinetic and imaging profiles compared with ^{11}C-GR103545.

MATERIALS AND METHODS

Chemistry

EKAP (compound **12**), its fumarate salt (compound **13**), and its optically pure precursor, (*S*)-**11,** were prepared from D-serine methyl ester according to a modification of a published procedure (*15*). The reaction schemes and conditions are shown in Figure 2. Detailed procedures for synthesis and characterization of compounds are included in the supplemental materials, available at http://jnm.snmjournals.org.

Radioligand Competition Binding Assays In Vitro

The 2 enantiomers (compounds **13** and **15**) were submitted to the National Institute of Mental Health Psychoactive Drug Screening Program for assays of binding affinities to MOR, KOR, and DOR following previously described procedures (https://pdspdb.unc.edu/pdspWeb/?site=assays). Each compound was assayed in triplicate.

Radiochemistry

^{11}C-EKAP (^{11}C-**12**) and its optically opposite enantiomer, ^{11}C-**14,** were prepared from precursors (*S*)-**11** and (*R*)-**11,** respectively, which were pretreated with CO_2, following a previously published procedure (*27*) with some modifications. The reaction conditions are shown in Figure 3. Detailed radiosynthetic procedures are included in the supplemental materials.

PET Imaging Experiments on Rhesus Monkeys

Monkey PET Scan Procedures. PET imaging experiments were performed in rhesus monkeys (*Macaca mulatta*) according to a protocol approved by the Yale University Institutional Animal Care and Use Committee. In preparation for each scan, the monkey was fasted overnight and immobilized with ketamine (10 mg/kg, intramuscularly) at least 2 h before the PET scan. A venous line was inserted into one limb for administration of radiotracer and blocking drug. A catheter was placed in the femoral artery in the other limb for blood sampling. Endotracheal intubation was performed to allow administration of isoflurane (1.5%–2.5% in oxygen). A water-jacket heating pad was used to maintain body temperature. The animal was attached to a physiologic monitor, and vital signs (heart rate, blood pressure, respirations, SPO_2, EKG, $ETCO_2$, and body temperature) were continuously

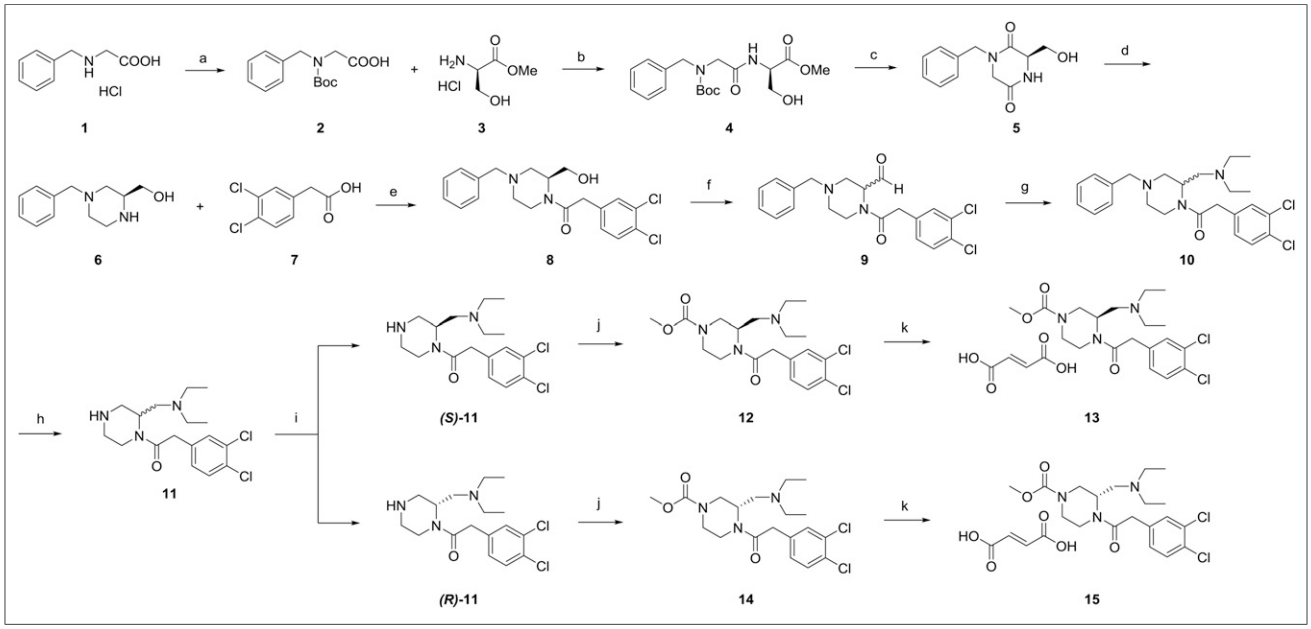

FIGURE 2. Synthetic scheme for EKAP and its corresponding ^{11}C-labeling precursors. Reagents and conditions: a. $(Boc)_2O$, triethylamine (TEA), H_2O, r.t., 3 h; b. *D*-Serine methyl ester hydrochloride (**3**), 1,1'-carbonyldiimidazole, TEA, CH_2Cl_2, 0°C to r.t., 16 h; c. $SOCl_2$, MeOH, r.t., 4 h then NH_4OH, MeOH, r.t., 16 h; d. $LiAlH_4$, THF, 60°C, 2 h; e. 3,4-Dichlorophenylacetic acid (**7**), 1,1'-carbonyldiimidazole, CH_2Cl_2, 0 °C to r.t., 16 h; f. Oxalyl chloride, DMSO, TEA, CH_2Cl_2, −78°C to r.t., 2 h; g. Diethylamine, $NaBH(OAc)_3$, $(CH_2Cl)_2$, 0°C then r.t., 16 h; h. Pd/C (10%), HCl, H_2, THF/H_2O, r.t., 4 h; i. Chiral separation; j. Methyl chlorofomate, TEA, CH_2Cl_2, r.t., 16 h; k. Fumaric acid, MeOH/Et_2O, 0°C, 5 min.

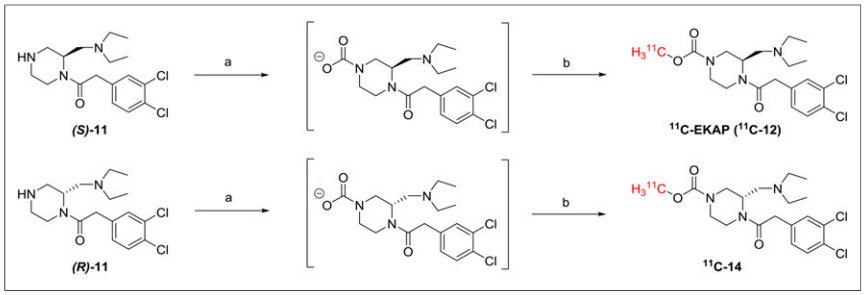

FIGURE 3. Radiosynthesis of ^{11}C-EKAP (**12**) and ^{11}C-**14**. Reagents and conditions: a. CO_2 (25 mL/min), cesium carbonate, tetrabutylammonium triflate, DMF, r. t., 5 min; b. ^{11}C-methyl triflate, 45 °C, 5 min.

monitored. Three monkeys were used in a total of 13 scans on a Focus 220 scanner (Siemens Medical Solutions). Among them, 10 scans with ^{11}C-**12** (^{11}C-EKAP) were obtained, including 5 baseline scans to assess kinetic and binding profiles, 5 blocking scans with the OR antagonist naloxone at 1 mg/kg dose (n = 2), and the KOR antagonist LY2795050 (0.2 mg/kg) and LY2456302 (0.3 and 0.05 mg/kg doses, respectively) to evaluate in vivo binding specificity and selectivity. One baseline scan with the inactive enantiomer ^{11}C-**14** and 2 scans with ^{11}C-GR103545 in 2 of the 3 monkeys were also acquired for comparison purposes. In the blocking scans, the blocking agents were given as a 3-min slow bolus injection at 20 min before radiotracer administration. A transmission scan was acquired before each PET scan for attenuation correction of PET data. Emission data were collected in list mode for 120 min and reformatted into 33 successive frames of increasing durations (6 × 30 s, 3 × 1 min, 2 × 2 min, and 22 × 5 min).

Plasma Metabolite Analysis and Input Function Measurement. Arterial blood samples were collected at preselected time points and assayed for radioactivity in whole blood and plasma with γ-counters (Wizard 1480/2480; Perkin Elmer). The unmetabolized parent fraction was determined as the ratio of the sum of radioactivity in fractions containing the parent compound to the total amount of radioactivity collected, fitted with an inverted γ-function and corrected for filtration efficiency. The arterial input function was calculated as the product of the total counts in the plasma and the interpolated parent fraction at each time point. Detailed procedures are included in the supplemental materials.

Measurement of Radiotracer Free Fraction in Plasma. An ultrafiltration method was used for measuring the unbound portion of ^{11}C-EKAP in plasma as previously described (*31*). The free fraction in plasma was determined as the ratio of the radioactivity concentration in the filtrate to the total activity in plasma. The free fraction was measured in triplicate for each scan.

Measurement of Lipophilicity. Lipophilicity (log*P*) was determined as previously described (*31*). log*P* was calculated as the ratio of decay-corrected radioactivity concentrations in 1-octanol and in phosphate-buffered saline (pH 7.4, Dulbecco). Six consecutive equilibration procedures were performed until a constant value of log*P* was obtained.

Image Analysis and Kinetic Modeling. High-resolution MR images were acquired with a Siemens 3-T Trio scanner to assist with image coregistration and anatomic localization of regions of interest (ROIs). The MR images were registered to an atlas and to the PET images.

PET emission data were attenuation-corrected using the transmission scan, and dynamic images were reconstructed using a Fourier rebinning and filtered backprojection algorithm. For each PET scan, time–activity curves (TACs) were generated for the ROIs. The ratio of tissue to metabolite-corrected plasma arterial input function over time was calculated for the cingulate cortex, temporal cortex, and cerebellum regions to project the radiotracer equilibration–approaching time.

Regional TACs were fitted and analyzed with the 1-tissue- and 2-tissue-compartment (1TC and 2TC, respectively) models (*32*), as well as the multilinear analysis 1 (MA1) method, with a starting time of 30 min (*33*). Regional distribution volume (V_T, mL/cm^3) was calculated from kinetic analysis of regional TACs using the metabolite-corrected arterial input function (*34*). The Akaike information criterion (*35*) and visual assessment of fitting curves (supplemental materials, Fig. 3A) were used to evaluate the goodness of fits.

Nondisplaceable binding potential (BP_{ND}) was calculated from regional V_T using the cerebellum as the reference region, that is, $BP_{ND} = (V_{T\ ROI} - V_{T\ cerebellum})/V_{T\ cerebellum}$. Additionally, the simplified reference tissue model (SRTM) was tested in calculating BP_{ND} to assess the possible generation of binding parameters without arterial blood samples (*36*).

KOR occupancy by the blocking drugs was obtained from occupancy plots using regional V_T from the baseline scan and the V_T difference between baseline and blocking scans (*37*).

RESULTS

Chemistry

The synthesis of EKAP (**12**) and of the precursor for ^{11}C-EKAP was adapted from the synthesis of GR103545 (*15*) and is depicted in Figure 2. The racemic compound **11** was prepared in 8 steps in an overall yield of 3%. The 2 enantiomers were separated by semipreparative chiral high-performance liquid chromatography (HPLC). Both the (*S*)-enantiomer ((*S*)-**11**) and the (*R*)-enantiomer ((*R*)-**11**) were obtained in greater than 95% chemical purity and over 99% enantiomeric purity, as indicated by analytic chiral HPLC (supplemental materials). (*S*)-**11** and (*R*)-**11** were used as precursors for radiolabeling and also were converted to the final compounds (**12**, or EKAP, and **14**), which were formulated as fumarate salts (**13** and **15**) for use in binding assays, and as reference standards in quality control analysis of the radiolabeled compounds.

In Vitro Binding Assays

The inhibition constant (K_i) for EKAP (**12**) (n = 3) was measured at 0.28 ± 0.03 nM for KOR, 8.6 ± 1.1 nM for MOR, and 386 ± 50 nM for DOR. The other enantiomer (**14**) displayed much lower affinities (13.0 ± 2.7 nM for KOR, 498 ± 39 nM for MOR, and >10,000 nM for DOR).

Radiochemistry

^{11}C-EKAP was prepared in 11% ± 3% radiochemical yield (decay-uncorrected), greater than 99% radiochemical purity, and a mean molar activity of 914 GBq/μmol at the end of synthesis (n = 12). The total synthesis time was about 47 min, including purification and formulation from the end of bombardment.

^{11}C-**14** was prepared from the corresponding precursor ((*R*)-**11**) in 11% radiochemical yield (decay-uncorrected), greater than 99% radiochemical purity, and 1,466 GBq/μmol molar activity at the end of synthesis (n = 1).

PET Imaging Experiments on Rhesus Monkeys

Injection Parameters. In total, 11 PET scans with ^{11}C-EKAP were performed on 3 monkeys. Injected activity was 155.7 ± 35.6 MBq, with an injected mass of 0.17 ± 0.08 μg.

Plasma Analysis. Results from plasma analysis are shown in Supplemental Figure 1. Metabolism of ^{11}C-EKAP was rapid, with 26% ± 6% of intact parent tracer at 30 min after injection, which

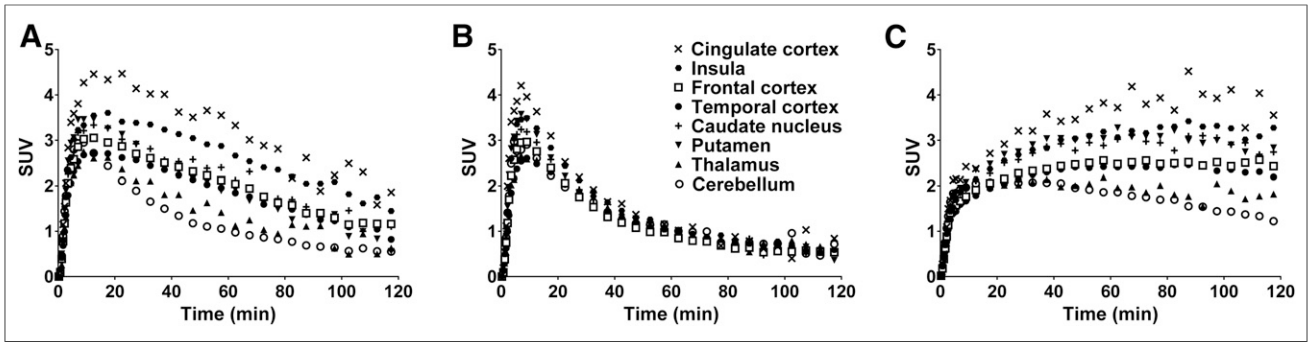

FIGURE 4. Brain regional TACs from baseline scans of ^{11}C-EKAP (A) and ^{11}C-**14** (B), in comparison with baseline scan of ^{11}C-GR103545 (C).

further decreased to 13% ± 4% and 9% ± 3%, respectively, at 60 and 90 min (n = 10). The other enantiomer, ^{11}C-**14,** showed a similar metabolism rate, with 18%, 9%, and 5% of parent at 30, 60, and 90 min after injection, respectively, whereas ^{11}C-GR103545 displayed a slower metabolism rate, with 44% ± 5% (n = 2) of parent fraction at 30 min. After a bolus injection of ^{11}C-EKAP, parent radioactivity level in plasma peaked quickly, sharply declined, and then slowly decreased from 10 min onward. On the reverse-phase HPLC, the 2 major metabolites of ^{11}C-EKAP appeared to be more polar, with retention time of 0.5 and 6.5 min, compared with 11.0 min for the parent. The measured log$P$ of ^{11}C-EKAP was 2.19 ± 0.06 (n = 6), slightly higher than that of ^{11}C-GR103545 (1.82 ± 0.02, n = 12). The ^{11}C-EKAP free fraction in plasma was 40% ± 10% (n = 5), similar to that of ^{11}C-GR103545 (42% ± 6%, n = 2).

Brain Analysis. Regional TACs from baseline scans of both ^{11}C-EKAP and ^{11}C-**14** are shown in Figure 4. As expected, ^{11}C-**14** displayed homogeneous regional uptake (Fig. 4B), indicating a lack of specific binding for the (*S*)-enantiomer and chirality of radiotracer binding. In comparison with ^{11}C-GR103545 in the same monkey (Fig. 4C), the tissue kinetics of ^{11}C-EKAP was much faster.

Shown in Figure 5 are representative PET images summed from 20 to 40 min after injection of ^{11}C-EKAP and the corresponding regional TACs in a baseline scan and blocking scans with naloxone (1 mg/kg) and LY2795050 (0.2 mg/kg). In the monkey brain, ^{11}C-EKAP exhibited heterogeneous distribution (Figs. 5A and 5B), and blocking with naloxone significantly reduced the binding of the radiotracer (Figs. 5A and 5C). Brain uptake of ^{11}C-EKAP was high, with an SUV_{peak} of 4.5 in the cingulate cortex (Fig. 5B). After entering the monkey brain, the radiotracer localized to KOR-rich regions. The highest concentrations were in cortical areas, whereas uptake was lowest in the cerebellum. Tissue kinetics of ^{11}C-EKAP was rapid and reversible. Regional concentrations of the radiotracer peaked within 20 min after injection, followed by a moderate rate of clearance over time. Pretreatment of the animal with naloxone and LY2795050 brought regional uptake levels in high-binding regions to the level in the cerebellum (Figs. 5C and 5D), demonstrating the binding specificity and selectivity of ^{11}C-EKAP. Blocking with the KOR-selective antagonist LY2456302 at 2 different doses (0.05 and 0.3 mg/kg) reduced the regional concentrations of ^{11}C-EKAP in a dose-dependent fashion (Supplemental Fig. 2), thus indicting the saturability of ^{11}C-EKAP binding.

Regional ratios of brain to metabolite-corrected plasma ^{11}C-EKAP activity are depicted in Figure 6A for 3 selected regions with low, medium, and high KOR densities. A steady state was achieved in all 3 regions at around 70 min after tracer injection. In contrast, the tissue-to-plasma ratio of ^{11}C-GR103545 (Fig. 6B) approached equilibrium in the region with low KOR density (cerebellum) only at the end of the 120-min scan but kept rising in the other 2 regions, further underscoring the much faster tissue kinetics and equilibrium of ^{11}C-EKAP than of ^{11}C-GR103545.

Regional TACs were processed with the 1TC and 2TC models and the MA1 method to generate binding parameters using the metabolite-corrected arterial input function. The 2TC model showed better fits of the TACs than the 1TC model (Akaike information criterion 2TC < Akaike information criterion 1TC). Regional V_T estimated with the MA1 method correlated well with that from 2TC ($V_{T\ MA1}$ = 1.0 $V_{T\ 2TC}$ − 0.34, r^2 = 1.00). However, the 2TC model

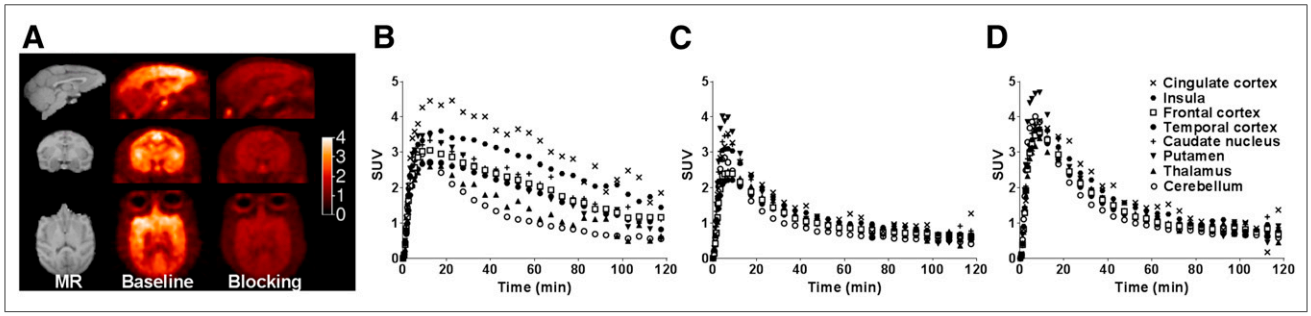

FIGURE 5. (A) MR (left) and summed PET SUV images from 20 to 40 min after ^{11}C-EKAP injection from baseline scan (middle), and blocking scan (right) with naloxone (1 mg/kg). (B–D) Brain regional TACs of ^{11}C-EKAP from baseline scan (B), and blocking scans with naloxone, 1 mg/kg (C), and LY2795050, 0.2 mg/kg (D).

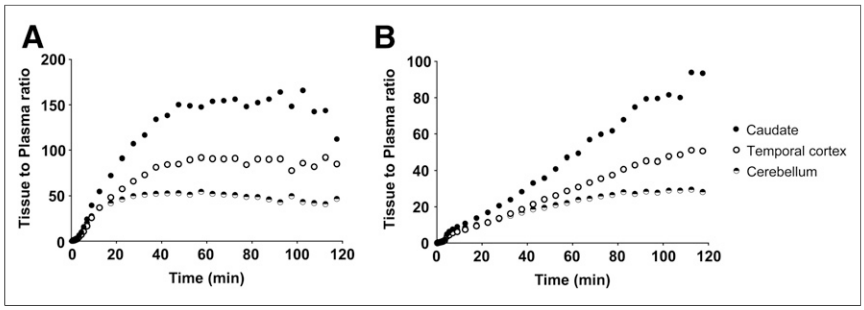

FIGURE 6. Comparison of tissue-to-plasma ratios over time from baseline scans with ^{11}C-EKAP (A) and ^{11}C-GR103545 (B) in same monkey.

sometimes produced implausible V_T values. Listed in Table 1 are regional V_T values derived from MA1 analysis (starting time, 30 min). Note that the other enantiomer, ^{11}C-**14,** exhibited V_T values largely indistinguishable among the brain regions, reflecting nonspecific binding.

Regional BP_{ND} was calculated from MA1 V_T using cerebellum as the reference region, along with those calculated from SRTM (Table 2). The rank order of BP_{ND} is as follows: cingulate cortex > globus pallidus > insula > caudate > putamen > frontal cortex > temporal cortex > thalamus > cerebellum, which is consistent with the reported KOR distribution in monkey brain (*29,38*). SRTM BP_{ND} correlated well with that of MA1 ($BP_{ND\ SRTM} = 0.91\ BP_{ND\ MA1} + 0.15$, $r^2 = 0.99$; supplemental materials, Fig. 3B).

Pretreatment with blocking agents significantly reduced regional V_T and brought BP_{ND} to negligible levels across brain regions. Using the MA1-derived V_T, receptor occupancy was calculated to be 86% ± 2% with a 1 mg/kg dose of naloxone ($n = 2$) and 89% with a 0.2 mg/kg dose of LY2795050. The other KOR-selective antagonist, LY2456302, induced 66% and 91% receptor occupancy at the 0.05 mg/kg and 0.3 mg/kg doses, respectively. The nondisplaceable distribution volume was derived from the occupancy plots, with a mean value of 10.2 mL/cm^3 ($n = 5$).

Comparison of ^{11}C-EKAP with ^{11}C-GR103545. Regional TACs from the baseline scans of ^{11}C-EKAP and ^{11}C-GR103545 are shown in Figure 4. Levels of regional brain uptake and distribution pattern were similar for these 2 radiotracers. ^{11}C-GR103545 had much slower tissue kinetics but higher binding parameters (V_T and BP_{ND}) than ^{11}C-EKAP (Table 3).

DISCUSSION

In this study, we developed and performed an in vivo evaluation of a KOR agonist PET radiotracer, ^{11}C-EKAP, in rhesus monkeys and compared it with ^{11}C-GR103545. The impetus for this study was to look for a KOR agonist radiotracer with faster kinetics than ^{11}C-GR103545, which has been shown in human studies to have very slow kinetics leading to poor test–retest variability of binding parameters in quantitative kinetic modeling. Along with our recently developed KOR antagonist PET radiotracers (*31*), the availability of a suitable agonist radiotracer will enable us to assess the ratio of receptors configured in the active versus inactive state and to investigate the possible receptor state change under diseased conditions (*25*).

The open-ring *N,N*-diethyl analog of GR103545, EKAP, and its ^{11}C-radiolabeling precursor were prepared in good yield. The 2 enantiomers of the racemic precursor were resolved by chiral HPLC with greater than 99% enantiomeric excess. ^{11}C-EKAP and ^{11}C-**14** were produced from the enantiomerically pure precursors with good radiochemical yield, purity, and molar activity at the end of synthesis.

In rhesus monkeys, ^{11}C-EKAP was metabolized at a rapid rate (Supplemental Fig. 1A). Two major radioactive metabolites were detected in the blood and appear to be much more polar than the parent radiotracer (Supplemental Fig. 1C) and, thus, are unlikely to enter the brain and complicate the quantitative analysis of PET imaging data. The free fraction in plasma is high (40%) and can be reliably measured.

^{11}C-EKAP has a measured log*P* of 2.19, in the range that is predicted to have good permeability through the blood–brain barrier (*39*). Indeed, ^{11}C-EKAP readily entered the monkey brain and accumulated in regions known to have high KOR densities, such as the cortex and striatum. Regional TACs demonstrated fast and reversible brain uptake kinetics. The highest tissue uptake levels were found in the globus pallidus and cingulate cortex. Peak uptake was reached within 20 min after injection in all brain regions. A baseline scan of the inactive enantiomer, ^{11}C-**14,** displayed only nonspecific binding, consistent with its low binding affinity to cloned human KOR (K_i = 13 nM vs. 0.28 nM for

TABLE 1
MA1-Derived V_T (mL/cm^3) of ^{11}C-EKAP in Monkey Brain

Parameter	Cingulate cortex	Globus pallidus	Insula	Caudate nucleus	Frontal cortex	Putamen	Temporal cortex	Thalamus	Cerebellum
Baseline ($n = 5$)	36.1 ± 7.7	36.5 ± 4.8	32.4 ± 6.7	24.6 ± 3.8	23.7 ± 8.2	22.6 ± 5.0	21.7 ± 4.7	16.8 ± 5.3	13.1 ± 2.2
^{11}C-**14** baseline	17.9	15.1	17.6	15.9	14.9	16.3	15.2	16.1	14.7
Naloxone blocking (1 mg/kg, $n = 2$)	12.0 ± 0.2	11.8 ± 0.2	11.9 ± 0.3	10.6 ± 0.4	10.2 ± 0.4	10.8 ± 0.1	9.6 ± 0.5	9.4 ± 0.1	8.6 ± 0.6
LY2795050 blocking (0.2 mg/kg)	13.7	11.9	12.6	11.7	11.1	12.0	10.5	10.9	10.0
LY2456302 blocking (0.05 mg/kg)	21.5	16.7	18.6	15.6	15.8	15.4	14.5	14.7	12.7
LY2456302 blocking (0.3 mg/kg)	15.7	14.7	15.5	14.3	14.7	16.4	12.4	13.6	12.9

TABLE 2
MA1- and SRTM-Derived Regional BP_{ND} of ^{11}C-EKAP in Monkey Brain

Parameter	Cingulate cortex	Globus pallidus	Insula	Caudate nucleus	Frontal cortex	Putamen	Temporal cortex	Thalamus
MA1								
Baseline (n = 5)	1.74 ± 0.17	1.79 ± 0.18	1.46 ± 0.14	0.88 ± 0.05	0.77 ± 0.29	0.71 ± 0.10	0.65 ± 0.10	0.26 ± 0.17
Naloxone blocking (1 mg/kg, n = 2)	0.39 ± 0.07	0.37 ± 0.11	0.38 ± 0.06	0.24 ± 0.14	0.19 ± 0.03	0.26 ± 0.10	0.11 ± 0.02	0.09 ± 0.06
LY2795050 blocking (0.2 mg/kg)	0.37	0.19	0.26	0.17	0.11	0.20	0.05	0.09
LY2456302 blocking (0.05 mg/kg)	0.70	0.32	0.47	0.24	0.25	0.22	0.15	0.16
LY2456302 blocking (0.3 mg/kg)	0.22	0.15	0.20	0.11	0.14	0.28	−0.04	0.06
SRTM								
Baseline (n = 4)	1.62 ± 0.16	1.40 ± 0.07	1.32 ± 0.14	0.83 ± 0.04	0.71 ± 0.28	0.69 ± 0.10	0.59 ± 0.09	0.25 ± 0.16
Naloxone blocking (1 mg/kg, n = 2)	0.42 ± 0.05	0.23 ± 0.12	0.38 ± 0.05	0.27 ± 0.10	0.15 ± 0.02	0.09 ± 0.15	0.12 ± 0.01	0.15 ± 0.06
LY2795050 blocking (0.2 mg/kg)	0.39	0.20	0.26	0.14	0.10	0.23	0.05	0.12
LY2456302 blocking (0.05 mg/kg)	0.47	0.18	0.28	0.55	−0.02	0.49	0.06	0.34
LY2456302 blocking (0.3 mg/kg)	−1.00	0.18	0.30	0.20	0.25	0.31	0.04	0.14

EKAP). In the blocking study, pretreatment with the nonselective opioid receptor antagonist naloxone (K_i = 2 nM for KOR) (*40*) induced significant reductions of regional difference in brain uptake, demonstrating the binding specificity of ^{11}C-EKAP. A blocking study with the KOR-selective antagonist LY2795050 (K_i = 0.72 nM for KOR) (*41*) reduced uptake of ^{11}C-EKAP across all ROIs to a similar level in the cerebellum and confirmed its binding selectivity for KOR. Further, dose-dependent blockade of specific binding was observed with LY2456302 (K_i = 0.81 nM for KOR) (*42*), indicating the saturability of ^{11}C-EKAP binding. Taken together, the experiments on rhesus monkeys demonstrated that binding of ^{11}C-EKAP in the brain is saturable, specific, and selective for KOR.

In a comparison of kinetic models for PET data analysis, the 2TC model provided good fits to regional TACs and was considered to be an appropriate model for estimation of binding parameters. Further comparison between the 2TC and MA1 methods revealed that MA1 produced reliable regional V_T estimates well correlated with those from 2TC, a finding that is consistent with previous kinetic model analysis of PET imaging data from other KOR radiotracers in nonhuman primates (*29*). The MA1 method was thus used to generate binding parameters. Regional V_T values in the ROIs showed high binding in the cortical and striatal regions and low binding in cerebellum, consistent with the KOR autoradiography results (*43*).

Previous studies with KOR radiotracers indicated that cerebellum can be used as a reference region in nonhuman primates to calculate BP_{ND} (*44*). This appeared to be true as well for ^{11}C-EKAP, as cerebellum V_T remained similar when various blocking drugs were administered and regional BP_{ND} values estimated by SRTM using cerebellum as the reference region exhibited an

TABLE 3
Comparison of Binding Parameters Derived from MA1 Between Baseline Scans of ^{11}C-EKAP and ^{11}C-GR103545 in Same Monkeys

Parameter	Cingulate cortex	Globus pallidus	Insula	Caudate nucleus	Frontal cortex	Putamen	Temporal cortex	Thalamus	Cerebellum
V_T (mL·cm^{-3})									
^{11}C-EKAP (n = 3)	32.7 ± 3.7	34.3 ± 1.2	29.0 ± 2.7	22.9 ± 1.5	20.4 ± 2.6	19.8 ± 1.7	19.7 ± 1.1	14.5 ± 1.4	12.1 ± 0.9
^{11}C-GR103545 (n = 2)	67.2 ± 19.2	46.6 ± 10.4	46.8 ± 10.4	37.8 ± 4.9	32.0 ± 4.1	33.5 ± 7.0	29.9 ± 3.5	18.6 ± 3.2	15.4 ± 2.0
BP_{ND}									
^{11}C-EKAP (n = 3)	1.70 ± 0.20	1.84 ± 0.24	1.40 ± 0.15	0.89 ± 0.07	0.68 ± 0.12	0.64 ± 0.02	0.63 ± 0.08	0.20 ± 0.03	—
^{11}C-GR103545 (n = 2)	3.33 ± 0.70	2.01 ± 0.29	2.03 ± 0.29	1.46 ± 0.01	1.08 ± 0.00	1.17 ± 0.18	0.94 ± 0.02	0.21 ± 0.06	—

excellent correlation with those derived from MA1 V_T. In Table 1, the V_T reduction in the cerebellum in the naloxone-blocking scans is likely due to the monkey-to-monkey difference, since the V_T average for the baseline scans included the third monkey with about 50% higher V_T (including cerebellum V_T) than the other 2 monkeys used in the naloxone-blocking scans.

Compared with ^{11}C-GR103545, ^{11}C-EKAP presented a similar plasma free fraction, brain uptake, and distribution pattern. On the other hand, ^{11}C-EKAP displayed a faster metabolism rate and tissue kinetics. Tissue-to-plasma ratios manifested a much earlier equilibrium stage with ^{11}C-EKAP than with ^{11}C-GR103545. The difference in specific binding signals as measured by BP_{ND} is small between ^{11}C-EKAP and ^{11}C-GR103545, and both ^{11}C-EKAP and ^{11}C-GR103545 provide a BP_{ND} of more than 0.5 in most brain regions, a level of specific binding signal that can be reliably and accurately estimated by quantitative kinetic modeling analysis and one of the important characteristics for a suitable and effective neuroimaging radiotracer (*45*).

CONCLUSION

We have successfully developed the KOR agonist PET radiotracer ^{11}C-EKAP and performed a detailed evaluation in nonhuman primates. This radiotracer exhibits favorable metabolic, pharmacokinetic, and in vivo binding profiles. A side-by-side comparison between ^{11}C-EKAP and ^{11}C-GR103545 indicates similarly high specific binding signals but a faster tissue kinetics with ^{11}C-EKAP. Given the desirable characteristics of this radiotracer, its evaluation in humans is warranted.

DISCLOSURE

The study was supported by grants from the National Institute of Mental Health (R21MH092664 and R33MH092664). No other potential conflict of interest relevant to this article was reported.

ACKNOWLEDGMENTS

We thank the staff at the Yale PET Center for their expert technical assistance.

REFERENCES

1. Martin WR, Eades CG, Thompson JA, Huppler RE, Gilbert PE. The effects of morphine- and nalorphine-like drugs in the nondependent and morphine-dependent chronic spinal dog. *J Pharmacol Exp Ther.* 1976;197:517–532.
2. Minami M, Satoh M. Molecular biology of the opioid receptors: structures, functions and distributions. *Neurosci Res.* 1995;23:121–145.
3. Hiller JM, Fan LQ. Laminar distribution of the multiple opioid receptors in the human cerebral cortex. *Neurochem Res.* 1996;21:1333–1345.
4. Simonin F, Gaveriaux-Ruff C, Befort K, et al. Kappa-opioid receptor in humans: cDNA and genomic cloning, chromosomal assignment, functional expression, pharmacology, and expression pattern in the central nervous system. *Proc Natl Acad Sci USA.* 1995;92:7006–7010.
5. Tejeda HA, Shippenberg TS, Henriksson R. The dynorphin/kappa-opioid receptor system and its role in psychiatric disorders. *Cell Mol Life Sci.* 2012;69:857–896.
6. McLaughlin JP, Marton-Popovici M, Chavkin C. Kappa opioid receptor antagonism and prodynorphin gene disruption block stress-induced behavioral responses. *J Neurosci.* 2003;23:5674–5683.
7. Newton SS, Thome J, Wallace TL, et al. Inhibition of cAMP response element-binding protein or dynorphin in the nucleus accumbens produces an antidepressant-like effect. *J Neurosci.* 2002;22:10883–10890.
8. Vonvoigtlander PF, Lahti RA, Ludens JH. U-50,488: a selective and structurally novel non-Mu (kappa) opioid agonist. *J Pharmacol Exp Ther.* 1983;224:7–12.
9. Loacker S, Sayyah M, Wittmann W, Herzog H, Schwarzer C. Endogenous dynorphin in epileptogenesis and epilepsy: anticonvulsant net effect via kappa opioid receptors. *Brain.* 2007;130:1017–1028.
10. Chappell PB, Leckman JF, Scahill LD, Hardin MT, Anderson G, Cohen DJ. Neuroendocrine and behavioral effects of the selective kappa agonist spiradoline in Tourette's syndrome: a pilot study. *Psychiatry Res.* 1993;47:267–280.
11. Cai Z, Ratka A. Opioid system and Alzheimer's disease. *Neuromolecular Med.* 2012;14:91–111.
12. Von Voigtlander PF, Lewis RA. U-50,488, a selective kappa opioid agonist: comparison to other reputed kappa agonists. *Prog Neuropsychopharmacol Biol Psychiatry.* 1982;6:467–470.
13. Lahti RA, Mickelson MM, McCall JM, Von Voigtlander PF. [^{3}H]U-69593 a highly selective ligand for the opioid kappa receptor. *Eur J Pharmacol.* 1985;109:281–284.
14. Hayes AG, Birch PJ, Hayward NJ, et al. A series of novel, highly potent and selective agonists for the kappa-opioid receptor. *Br J Pharmacol.* 1990;101:944–948.
15. Naylor A, Judd DB, Lloyd JE, Scopes DI, Hayes AG, Birch PJ. A potent new class of kappa-receptor agonist: 4-substituted 1-(arylacetyl)-2-[(dialkylamino) methyl]piperazines. *J Med Chem.* 1993;36:2075–2083.
16. Chesis PL, Welch MJ. Synthesis and *in vitro* characterization of fluorinated U-50488 analogs for PET studies of kappa opioid receptors. *Int J Rad Appl Instrum [A].* 1990;41:267–273.
17. Noble G, Dannals RF, Ravert HT, Wilson AA, Wagner HN. Synthesis of a radiotracer for studying k-subtype opiate receptors: N-[^{11}C-methyl]-N-(trans-2-pyrrolidinyl-cyclohexyl)-3,4-dichlorophenylacetamide ([^{11}C]-(±)-U-50488H). *J Labelled Compd Radiopharm.* 1992;31:81–89.
18. Ravert HT, Mathews WB, Musachio JL, Scheffel U, Finley P, Dannals RF. [^{11}C]-methyl 4-[(3,4-dichlorophenyl)acetyl]-3-[(1-pyrrolidinyl)-methyl]-1-piperazine-carboxylate ([^{11}C]GR89696): synthesis and in vivo binding to kappa opiate receptors. *Nucl Med Biol.* 1999;26:737–741.
19. Ravert HT, Scheffel U, Mathews WB, Musachio JL, Dannals RF. [^{11}C]-GR89696, a potent kappa opiate receptor radioligand: *in vivo* binding of the *R* and *S* enantiomers. *Nucl Med Biol.* 2002;29:47–53.
20. Schmidt MD, Schmidt MS, Butelman ER, et al. Pharmacokinetics of the plant-derived kappa-opioid hallucinogen salvinorin A in nonhuman primates. *Synapse.* 2005;58:208–210.
21. Hooker JM, Xu Y, Schiffer W, Shea C, Carter P, Fowler JS. Pharmacokinetics of the potent hallucinogen, salvinorin A in primates parallels the rapid onset and short duration of effects in humans. *Neuroimage.* 2008;41:1044–1050.
22. Hooker JM, Munro TA, Beguin C, et al. Salvinorin A and derivatives: protection from metabolism does not prolong short-term, whole-brain residence. *Neuropharmacology.* 2009;57:386–391.
23. Yan F, Bikbulatov RV, Mocanu V, et al. Structure-based design, synthesis, and biochemical and pharmacological characterization of novel salvinorin A analogues as active state probes of the kappa-opioid receptor. *Biochemistry.* 2009;48:6898–6908.
24. Leff P. The two-state model of receptor activation. *Trends Pharmacol Sci.* 1995;16:89–97.
25. Finnema SJ, Bang-Andersen B, Wikstrom HV, Halldin C. Current state of agonist radioligands for imaging of brain dopamine D_2/D_3 receptors in vivo with positron emission tomography. *Curr Top Med Chem.* 2010;10:1477–1498.
26. Che T, Majumdar S, Zaidi SA, et al. Structure of the nanobody-stabilized active state of the kappa opioid receptor. *Cell.* 2018;172:55–67.
27. Nabulsi NB, Zheng MQ, Ropchan J, et al. [^{11}C]GR103545: novel one-pot radiosynthesis with high specific activity. *Nucl Med Biol.* 2011;38:215–221.
28. Naganawa M, Jacobsen LK, Zheng MQ, et al. Evaluation of the agonist PET radioligand [^{11}C]GR103545 to image kappa opioid receptor in humans: kinetic model selection, test-retest reproducibility and receptor occupancy by the antagonist PF-04455242. *Neuroimage.* 2014;99:69–79.
29. Tomasi G, Nabulsi N, Zheng MQ, et al. Determination of in vivo Bmax and Kd for ^{11}C-GR103545, an agonist PET tracer for kappa-opioid receptors: a study in nonhuman primates. *J Nucl Med.* 2013;54:600–608.
30. Talbot PS, Narendran R, Butelman ER, et al. ^{11}C-GR103545, a radiotracer for imaging kappa-opioid receptors in vivo with PET: synthesis and evaluation in baboons. *J Nucl Med.* 2005;46:484–494.
31. Li S, Cai Z, Zheng MQ, et al. Novel ^{18}F-labeled kappa-opioid receptor antagonist as PET radiotracer: synthesis and in vivo evaluation of ^{18}F-LY2459989 in nonhuman primates. *J Nucl Med.* 2018;59:140–146.
32. Gunn RN, Gunn SR, Cunningham VJ. Positron emission tomography compartmental models. *J Cereb Blood Flow Metab.* 2001;21:635–652.
33. Ichise M, Toyama H, Innis RB, Carson RE. Strategies to improve neuroreceptor parameter estimation by linear regression analysis. *J Cereb Blood Flow Metab.* 2002;22:1271–1281.
34. Innis RB, Cunningham VJ, Delforge J, et al. Consensus nomenclature for *in vivo* imaging of reversibly binding radioligands. *J Cereb Blood Flow Metab.* 2007;27:1533–1539.
35. Akaike H. New look at statistical-model identification. *IEEE Trans Autom Control.* 1974;19:716–723.
36. Lammertsma AA, Hume SP. Simplified reference tissue model for PET receptor studies. *Neuroimage.* 1996;4:153–158.

37. Cunningham VJ, Rabiner EA, Slifstein M, Laruelle M, Gunn RN. Measuring drug occupancy in the absence of a reference region: the Lassen plot re-visited. *J Cereb Blood Flow Metab.* 2010;30:46–50.
38. Sim-Selley LJ, Daunais JB, Porrino LJ, Childers SR. Mu and kappa1 opioid-stimulated [^{35}S]guanylyl-5′-O-(gamma-thio)-triphosphate binding in cynomolgus monkey brain. *Neuroscience.* 1999;94:651–662.
39. Seelig A, Gottschlich R, Devant RM. A method to determine the ability of drugs to diffuse through the blood-brain-barrier. *Proc Natl Acad Sci USA.* 1994;91:68–72.
40. Wang D, Sun XC, Sadee W. Different effects of opioid antagonists on mu-, delta-, and kappa-opioid receptors with and without agonist pretreatment. *J Pharmacol Exp Ther.* 2007;321:544–552.
41. Zheng MQ, Nabulsi N, Kim SJ, et al. Synthesis and evaluation of ^{11}C-LY2795050 as a kappa-opioid receptor antagonist radiotracer for PET imaging. *J Nucl Med.* 2013;54:455–463.
42. Rorick-Kehn LM, Witkin JM, Statnick MA, et al. LY2456302 is a novel, potent, orally-bioavailable small molecule kappa-selective antagonist with activity in animal models predictive of efficacy in mood and addictive disorders. *Neuropharmacology.* 2014;77:131–144.
43. Ragen BJ, Freeman SM, Laredo SA, Mendoza SP, Bales KL. mu and kappa opioid receptor distribution in the monogamous titi monkey (*Callicebus cupreus*): implications for social behavior and endocrine functioning. *Neuroscience.* 2015;290:421–434.
44. Zheng MQ, Kim SJ, Holden D, et al. An improved antagonist radiotracer for the kappa-opioid receptor: synthesis and characterization of ^{11}C-LY2459989. *J Nucl Med.* 2014;55:1185–1191.
45. Laruelle M, Slifstein M, Huang Y. Relationships between radiotracer properties and image quality in molecular imaging of the brain with positron emission tomography. *Mol Imaging Biol.* 2003;5:363–375.

Erratum

In the article "Three-Dimensional Dosimetry for Radiation Safety Estimates from Intrathecal Administration," by Hesterman et al. (*J Nucl Med.* 2017;58:1672–1678), the absorbed doses given in Table 3 and the in-text references to these values from Table 3 are incorrect. The correct values appear in italics in the paragraphs as well as the table below. Despite these errors, there is no impact to the methods, statistical analysis, or conclusions. The authors regret the error.

In the abstract:

Simulation results were within 6% of OLINDA estimates for common organs. Absorbed dose estimates were highest (*0.5–1.2* mGy/MBq) in the lumbar CSF space.

In the "Discussion: Clinical Data" section:

The lumbar CSF region experiences the highest exposure, with an absorbed dose per unit injected activity of approximately *1.2 ± 0.3* mGy/MBq for a 5-mL administered volume, with radiation dose decreasing along the spinal cord up to the brain. In the case of the 5-mL administration, the ratio of absorbed dose between lumbar and cervical CSF is approximately *6.0* and lumbar to brain tissue is about *32.* A more uniform distribution of absorbed dose is observed with the 15-mL dose volume with lumbar–to–cervical and lumbar–to–brain tissue ratios of about *2.3* and *10.3,* respectively. Additionally, the brain CSF, comprising largely the cisterns, and brain parenchyma doses are approximately 1.4 times higher in the 15-mL administered volume group than in the 5-mL group.

In the "Discussion: Biological Implications" section:

The current experimentally derived dosimetry after intrathecal administration indicates an absorbed dose per unit injected activity of up to *1.2* mGy/MBq in the lumbar spine (5-mL injection, $n = 3$ subjects). In this study, the administered activity of ^{99m}Tc was about 185 MBq, resulting in a total radiation dose of about *220* mGy (*0.22* Gy).

In Table 3:

TABLE 3
Absorbed Dose Per Unit Injected Activity for Regions of Interest (μGy/MBq)

Region	5 mL	15 mL
Brain	*36.39 ± 16.25*	*51.38 ± 4.40*
Right lung	*3.50 ± 0.27*	*2.73 ± 0.32*
Left lung	*3.37 ± 0.25*	*2.63 ± 0.30*
Liver	*3.19 ± 0.33*	*2.09 ± 0.12*
Kidneys	*14.12 ± 1.27*	*9.85 ± 0.47*
Stomach	*3.23 ± 0.34*	*2.15 ± 0.12*
Heart	*2.01 ± 0.10*	*1.47 ± 0.11*
Bladder	*4.73 ± 1.53*	*6.69 ± 3.74*
Cervical CSF	*195.75 ± 88.44*	*231.41 ± 39.79*
Thoracic CSF (upper)	*353.68 ± 84.83*	*277.66 ± 83.72*
Thoracic CSF (lower)	*470.37 ± 34.79*	*365.47 ± 23.88*
Lumbar CSF	*1,174.70 ± 283.85*	*527.40 ± 98.70*
Brain ventricle CSF	*23.31 ± 10.39*	*32.83 ± 2.79*
Entire body	*3.32 ± 0.24*	*2.88 ± 0.10*

*Statistically significant differences (lS t test, equal variance) observed between 5- and 15-mL groups.
Data are mean ± SD